DOI 10.1007/s11141-014-9529-2
Radiophysics and Quantum Electronics, Vol. 57, No. 7, December, 2014
(Russian Original Vol. 57, No. 7, July, 2014)

NUMERICAL SIMULATION OF THE INFLUENCE OF THE MAY 2–3, 2010 GEOMAGNETIC STORM ON HF RADIO-WAVE PROPAGATION IN THE IONOSPHERE

D. S. Kotova,[1,2] * **M. V. Klimenko,**[1,2] **V. V. Klimenko,**[1] **and V. E. Zakharov** [2]

UDC 550.388.2

This study is devoted to HF radio wave propagation in the ionosphere during the May 1–3, 2010 geomagnetic storm. The research results were obtained by using two models, namely, the GSM TIP environment model developed at WD IZMIRAN and the radio-wave propagation model developed at I. Kant BFU. For certain selected frequencies we show the effect of the geomagnetic storm on the radio wave propagation. We give examples of a HF radio-wave path in the channels between the F_1 and F_2 layers of a high-latitude ionosphere and the F_2 and F_3 layers of a low-latitude ionosphere. Characteristics of these layers may significantly affect the interpretation of the oblique sounding ionograms.

1. INTRODUCTION

Despite the long period of the ionospheric research using oblique sounding ionograms [1–3], the problem of interpreting some features of these ionograms still remains, especially in the periods of geomagnetic storms. This is due to the fact that there is no constant global monitoring of the three-dimensional ionospheric structure. The objective of this study is to demonstrate the capabilities of such an approach.

Until now, an empiric model of the ionosphere, which would correctly describe changes in the ionospheric parameters during geomagnetic storms has not yet been established. Even the International Reference Ionosphere (IRI) model [4]), which describes well the ionospheric behavior in a quiet geomagnetic environment does not reproduce ionospheric disturbances during storms [5, 6]. However, different three-dimensional global numerical models of the Earth's upper atmosphere describe these disturbances well enough [7–11]. In this paper, as a model of the medium, we used a global self-consistent model of the thermosphere, ionosphere, and protonosphere (GSM TIP model [12, 13]) developed in the Western Division of N. V. Pushkov Institute of Terrestrial Magnetism, Ionosphere and Radio Wave Propagation of the Russian Academy of Sciences (WD IZMIRAN). For a study of radio paths in the medium obtained using the GSM TIP model, we employed the radio-wave propagation model developed at the I. Kant Baltic Federal University (BFU) [14–17].

Over the last decade, the HF radio-wave propagation paths were studied by combining different numerical models of the ionosphere and radio-wave propagation [18–20]. In these papers, a model description of the radio-wave propagation in the region of the main ionospheric trough was developed [18], model oblique-sounding ionograms were constructed with the subsequent interpretation of experimental ionograms [19], and a model examination of the basic characteristics of the oblique sounding ionograms was performed [20].

* darshu@ya.ru

[1] Western Division of N. V. Pushkov Institute of Terrestrial Magnetism, Ionosphere and Radio Wave Propagation of the Russian Academy of Sciences (WD IZMIRAN), St. Petersburg; [2] I. Kant Baltic Federal University, Kaliningrad, Russia. Translated from Izvestiya Vysshikh Uchebnykh Zavedenii, Radiofizika, Vol. 57, No. 7, pp. 519–530, July 2014. Original article submitted February 10, 2014; accepted April 14, 2014.

However, these studies have constraints. Namely, they use either the model of a high-latitude ionosphere or the model of the ionosphere–plasmasphere system with the low-latitude region neglected. These models are not global three-dimensional ones and do not calculate self-consistently the electric field and the parameters of the thermosphere and ionosphere.

Our studies are specific in that the numerical calculation of the HF radio-wave propagation paths in three-dimensional inhomogeneous anosotropic dispersive regions of the low- and high-latitude ionosphere using the model of a medium for quiet geomagnetic conditions and in the different phases of a geomagnetic storm. The obtained results make it possible to analyze the influence of geomagnetic disturbances on the HF radio-wave propagation. During the processing of model calculations, we detected HF radio-wave propagation trajectories between the ionospheric layers in the low- and high-latitude ionosphere. Characteristics of these trajectories can significantly affect the interpretation of oblique-sounding ionograms.

2. BRIEF DESCRIPTION OF THE RADIO-WAVE PROPAGATION MODEL

As a numerical model of the radio-wave propagation with different carrier frequencies in an inhomogeneous anisotropic dispersive ionosphere, the model described in [14] is used. Note that for the description of the ray trajectories of radio waves in the ionosphere, a geometrical-optics approximation is applicable [21]. For each of the two normal modes, solving the eikonal equation by the method of characteristics reduces to the interpretation of a system of six ray equations for the coordinates and momenta. The numerical integration is performed by the Runge–Kutta method in a spherical geomagnetic coordinate system.

The refractive indices of the O and X modes at ionospheric altitudes of 60 to 1000 km are calculated using the dielectric-permittivty tensor of a cold plasma [22]. In order to test the algorithm, these refractive indices were also calculated based on the Appleton–Hartree formula. Comparison of the results of numerical calculations by both techniques showed a qualitative agreement between them. The model estimates the differential absorption coefficient for each of the two normal modes:

$$k[\mathrm{dB/m}] = 8.68\,(\omega[\mathrm{s}^{-1}]/\mathrm{s[m/s]})\,\mathrm{Im}\,n,$$

where ω is the oscillation frequency, c is the speed of light, and n is the refractive index of the medium.

Integral absorption along each ray on a length interval from σ_0 to σ is equal to

$$k_{\mathrm{int}} = \int\limits_{\sigma_0}^{\sigma} k\cos\gamma\,\mathrm{d}\sigma,$$

where γ is the angle between the momentum $\mathbf{p} \parallel \mathbf{k}$ and the tangent $\mathbf{s}$ of the ray and σ is the coordinate along the ray.

The chosen model is complex and universal. The model takes into account the three-dimensional heterogeneity, anisotropy, and dispersion of the propagation medium, the dependence of the parameters of the ionosphere and the neutral atmosphere on the solar and geophysical conditions. The presence of different output model parameters, for example, such as the group delay time, permitted one to compare the results of model calculations for the Murmansk–St. Petersburg radio path and the experimental data [14].

Earlier, a three-dimensional inhomogeneous anisotropic model of the radio-wave propagation medium was constructed by using empiric models of the ionosphere (e. g., IRI) and neutral atmosphere. However, as was shown in [6], the IRI model describes the disturbed medium insufficiently well. In this study, the parameters of the medium at ionospheric altitudes of 80 to 1000 km, which are used for calculation of the radio-wave refractive indices, were calculated for the first time using a global theoretical model of the thermosphere–ionosphere system (GSM TIP). This model describes the parameters of an inhomogeneous anisotropic medium both in quiet geomagnetic conditions and during geomagnetic storms. The radio-wave propagation model and the GSM TIP model were adapted for the first time in [23].

3. BRIEF DESCRIPTION OF THE GSM TIP MODEL

The GSM TIP model was developed in the ionospheric processes simulation laboratory of the Western Division of IZMIRAN. The model calculates time-dependent global three-dimensional distributions of the temperature, velocity, and number density of electrons, ions (O^+, H^+, N_2^+, O_2^+, and NO^+), and molecules (O_2, N_2, and O), as well as a two-dimensional distribution of the electric field of the ionospheric (dynamo field) and magnetospheric (magnetospheric convection field) origin. All equations of the model are solved by the finite differences technique. The geomagnetic field is approximated by the field of a point geomagnetic dipole located at the Earth's center. The model also takes into account the noncoincidence of the geographic and geomagnetic poles. In [13], the model was modified in terms of calculation of the electric fields, which permitted one to correctly describe the electric field at low altitudes and the geomagnetic equator, as well as the zonal currents in the Earth's ionosphere.

Papers [6, 10, 11, 24, 25] show the results of numerical calculations of the ionospheric effects of geomagnetic storms in the period from 2000 to 2011, which were obtained by using various modifications of the problem formulation in the GSM TIP model. The following was obtained: a mechanism for the formation of the F_3 layer and a multilayer structure in the ionospheric equatorial F region during geomagnetic storms has been explained; ionospheric effects of the electric field generation in disturbed conditions, the effects of direct penetration of the magnetospheric convection field to the mid- and low latitudes, and supershielding effects have been correctly singled out; mechanisms for the formation of the main and recovery phases of ionospheric storms have been examined. Comparison of the results of model calculations of various ionospheric parameters with observations of a high-, mid-, and low-latitude ionosphere, which is presented in these papers, has shown a satisfactory qualitative and sometimes also quantitative agreement, which confirms the feasibility of using the GSM TIP model.

In the model calculations presented in this paper, the cross-polar cap potential difference was specified through a geomagnetic activity index AE according to [26] using the formula $V[\mathrm{kV}] = 38 + 0.089AE[\mathrm{nT}]$ at the geomagnetic latitudes $\Phi = 75^\circ$ and $\Phi = -75^\circ$. Variations in the polar-cap sizes during the disturbances were neglected. Based on the results of experimental studies [27, 28] we constructed empiric dependences of the amplitudes of the region-2 field-aligned currents on the geomagnetic activity index AE: $j_2[\mathrm{A/m^2}] = 3 \cdot 10^{-8} + 1.2 \cdot 10^{-10} AE[\mathrm{nT}]$. According to [29], the time delay of variations in the region-2 field-aligned currents with respect to variations in the cross-polar cap potential difference (the delay is 30 min) was taken into account. The geomagnetic latitudes corresponding to the maxima of the region-2 field-aligned currents as functions of the cross-polar cap potential difference were set at different geomagnetic latitudes according to [30] and are presented in Table 1. Precipitation of energetic particles (energy flux and energy of particles) was specified according to the empiric model described in [31].

TABLE 1

V, kV	$\lvert\Phi\rvert$, degrees
$0 \le V \le 40$	65
$40 < V \le 50$	60
$50 < V \le 89$	55
$89 < V \le 127$	50
$127 < V \le 165$	45
$165 < V \le 200$	40
$V > 200$	35

4. THE MAY 2–3, 2010 GEOMAGNETIC STORM

In this study, we used the results of model calculations [24] of the ionospheric response to the May 2–3, 2010 geomagnetic storm, which were obtained in the GSM TIP model in the problem formulation described above. Figure 1 shows the behavior of the geomagnetic activity indices D_{st}, K_{p}, AL, and AE over the considered period of time of May 1–3, 2010. It is seen that the storm suddenly commenced at about 09:00 UT on May 2, 2010 followed by the main phase of the storm, which reached its maximum at 15:00 UT and changed to the recovery phase. The auroral electrojects were enhanced during the storm, as was indicated by the behavior of the AE index. The maximum value of the three-hour index K_{p} for this storm did not exceed 6. The indices K_{p} and AE were used for calculation of the input parameters

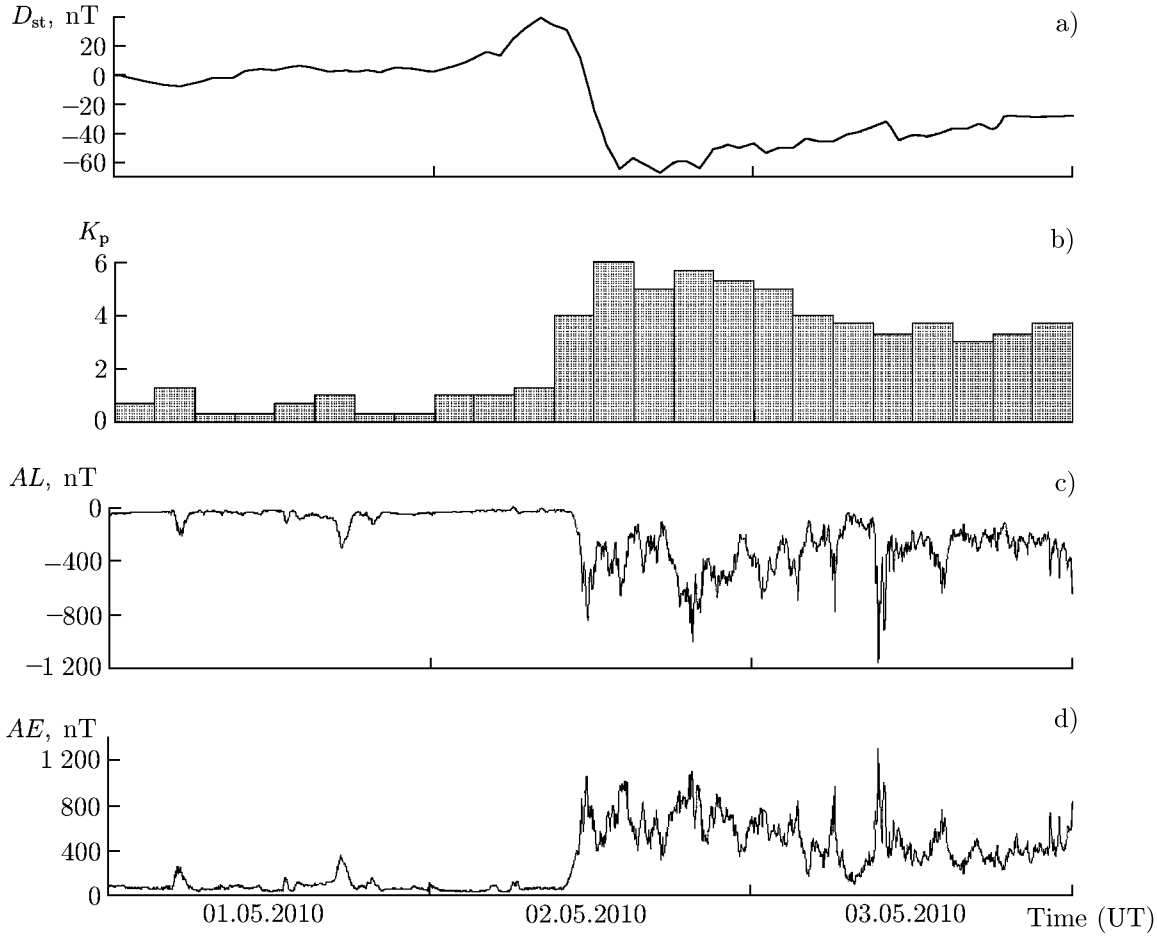

Fig. 1. Geomagnetic activity indices D_{st} (*a*), K_p (*b*), AL (*c*), and AE (*d*) on May 1–3, 2010.

of the model (the cross-polar cap potential difference, region-2 field-aligned currents, and auroral-electron precipitation) for the considered period of time.

The phenomenon being studied occurred at the minimum of the 24th solar activity cycle. The solar activity index $F_{10.7}$ changed during the storm from 77.8 to 80.3. The main mechanisms of the formation of an ionospheric response to this geomagnetic storm were considered in [32]. It was shown that, despite the global variations in the composition of the neutral atmosphere (a decrease in the density ratio of atomic oxygen and nitrogen), which decrease the cutoff frequency of the F_2 layer by about 40% at high latitudes, the appearance of additional wind in the equator direction increases the frequency f_{oF_2} at midlatitudes. The maximum wind disturbance is observed at high latitudes and the maximum increase in frequency f_{oF_2} (by about 20%), at midlatitudes. The maximum of the positive disturbances of the frequency f_{oF_2} shifts towards the midlatitudes because the inclination angle of the magnetic field decreases with the distance from the pole to the midlatitudes, and therefore the efficiency of the vertical plasma transport along the geomagnetic field lines increases due to the meridional component of thermospheric wind.

To test the results of model calculations, we compared them with the observation data of the vertical sounding stations in Kaliningrad (54.6° N, 20.2° E) and São José dos Campos (Brazil, 23.2° S, 45.9° W), which is shown in Fig. 2. It can be noted that the calculated cutoff frequency f_{oF_2} is slightly lower than the observed one, and the difference of the values is significantly smaller for the midlatitude station. The positive disturbances of May 2 in the period from 15:00 to 18:00 UT and of May 3 from 02:00 to 04:00 UT are seen in the behavior of the frequency f_{oF_2} over Kaliningrad. They can also be seen in the calculation results. The negative disturbances of May 2 in the period from 18:00 to 21:00 UT and of May 3 from 19:00 to 24:00 UT, especially from 08:00 to 15:00 UT, also agree well.

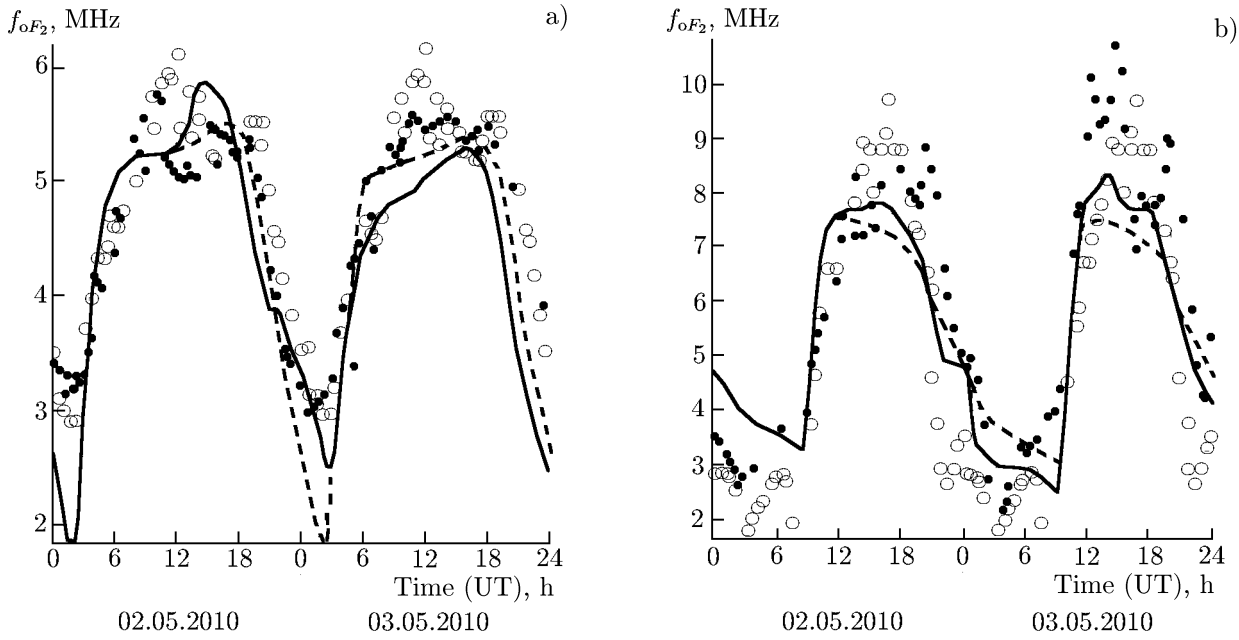

Fig. 2. Cutoff frequency f_{oF_2} during the May 2–3, 2010 geomagnetic storm over the Kaliningrad station (*a*) and the São José dos Campos station (*b*). The observation data are shown by light circles for the quiet day of May 1 and by dark circles for May 2 and 3. The results of model calculations are shown by dotted lines for quiet conditions and by solid lines for the disturbed days.

The results of calculations over the São José dos Campos station reproduces the observed positive effect in the daytime. On May 2, as in the experiment, this effect is smaller than on May 3. However, one should mention the differences in the disturbances of the frequency f_{oF_2} in the night time in the observation data and in the model calculation results. Despite this, it can be concluded that on the whole the results of model calculations reproduce well the observations both in quiet conditions and in the main and recovery phases of the May 2–3, 2010 storm.

5. THE RESULTS OF CALCULATIONS OF THE HF RADIO-WAVE PROPAGATION TRAJECTORIES

We have performed a number of numerical experiments on the radio-wave propagation modeling with a combination of the radio-wave propagation and GSM TIP models on May 1–3, 2010 for several hypothetic stations at high and low latitudes, sweeping the radiation frequencies, elevation angles, and azimuthal directions. Figures 3–5 show the most interesting results of calculating the trajectories for hypothetic transmitting radio stations located on the Earth's surface at low and high latitudes. All the figures presented above correspond to single-hop paths of the O-mode radio wave. The choice of time and propagation direction of radio waves is related to the fact that exactly at these instants and in these directions the electron-density inhomogeneities in the high- and low-latitude ionospheric F region are most clearly manifested.

The first station with the coordinates $\varphi = 10^\circ$ S, $\lambda = 69^\circ$ W; $\Phi = 1.4^\circ$, $\Lambda = 0.8^\circ$ (φ and λ are the geographic and Φ and Λ, geomagnetic latitude and longitude, respectively) is located in the equatorial region. The elevation angle of the transmitting antenna of this station is $\alpha = 45^\circ$. The antenna radiates radio waves in the easterly direction. Thus, the trajectories of the radio waves radiated by such a radio station are directed from the night- to the daytime side near the geomagnetic equator plane, i. e., in the region of the equatorial anomaly trough.

Figure 3 shows the trajectories of radio waves with three different frequencies against the electron-density isoline maps plotted in the radio-wave propagation plane. The calculation results are presented for 09:30 UT on May 1 and 3. In each of these maps one can see the formation of two maxima and a valley

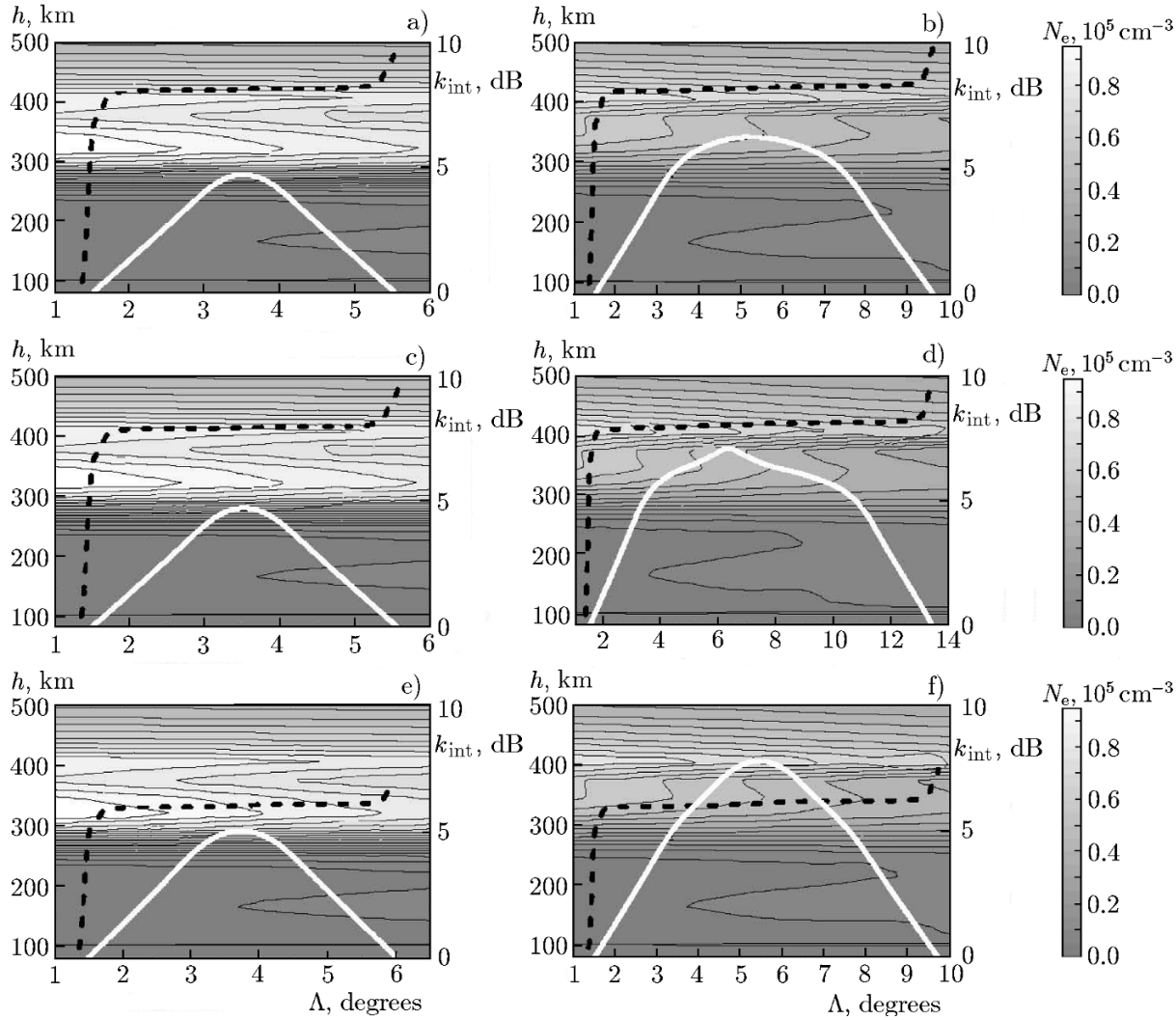

Fig. 3. Calculated trajectories (white lines) and integral dampings (dashed lines) of radio waves with the frequencies $f = 2.82$ MHz (*a* and *b*), $f = 2.86$ MHz (*c* and *d*), and $f = 3.35$ MHz (*e* and *f*) against the background of the electron density isolines constructed along the trajectories. The waves are radiated by the equatorial radio station. Quiet conditions (May 1, 09:30 UT) are represented on panels *a*, *c*, and *e* and the recovery phase of the storm (May 3, 09:30 UT), on panels *b*, *d*, and *f*.

between them in an altitude interval of about 300 to 400 km. This indicates the existence of an additional F_3 layer in the equatorial ionosphere at that time. It was shown before that the numerical models of the ionosphere reproduce the formation of the F_3 layer, which is observed in the equatorial ionosphere both in quiet conditions [33–35] and during geomagnetic storms [36].

From a comparison of the trajectories it is seen that in quiet conditions (May 1) and in the storm recovery phase (May 3) they strongly differ from each other. In a quiet environment, the altitude variation in the electron-density gradient is much stronger than in the recovery phase during which the electron number density in the equatorial plane decreases by 20–45% compared with quiet conditions. This fact decreases the maximum frequency at which the radio wave is retained in the waveguide and results in deeper penetration of the wave into the ionosphere. In the recovery phase of the storm, the wave with the frequency $f = 2.62$ MHz is reflected from the F_2 layer and the wave with $f = 3.35$ MHz, from the F_3 layer. It is also well seen that the wave with $f = 2.86$ MHz in quiet conditions is reflected from the F_2 layer, and during the storm the wave is first refracted in the F_2 layer and then is reflected from the F_3 layer and then is refracted again in the F_2 layer. Thus, the wave undergoes strong refraction in the F_2 and F_3 layers. The trajectories presented

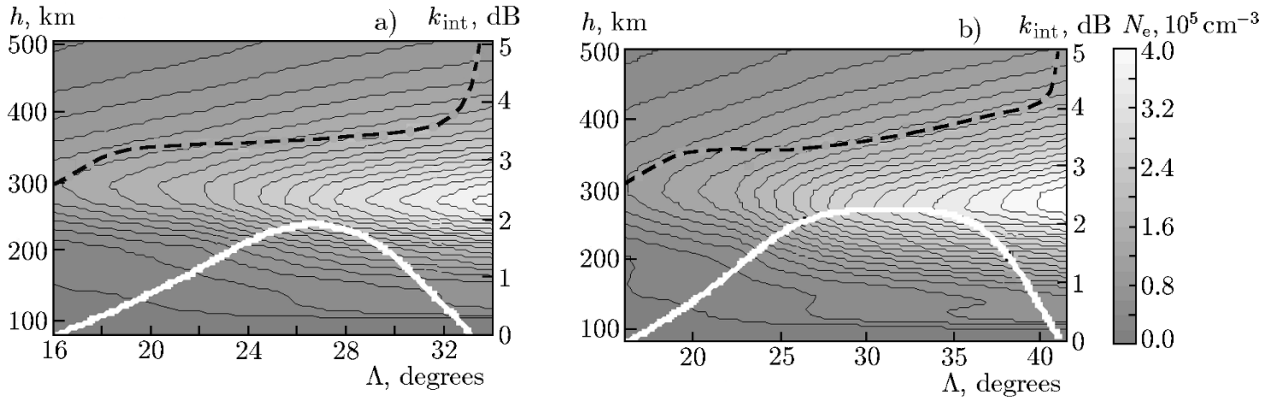

Fig. 4. The same as Fig. 3 but for the second equatorial radio station and the radio wave with the frequency $f = 12.96$ MHz (panel *a* corresponds to 09:30 UT May 1, 2010 and panel *b*, to 09:30 UT May 2, 2010).

in this paper show that the oblique sounding ionograms can be used for a study of the spatial extent of the additional F_3 layer and its variability during geomagnetic storms.

The second equatorial station has the coordinates $\varphi = 2^\circ$ N, $\lambda = 60^\circ$ W; $\Phi = 10.1^\circ$, $\Lambda = 13.2^\circ$, elevation angle of the transmitting antenna $\alpha = 5^\circ$; the radio waves are radiated in the easterly direction. Figure 4 presents the case of the Pedersen ray formation in the recovery phase of the storm. In quiet conditions, the wave is reflected at the lower altitudes since the electron number density reaches greater values. In disturbed conditions, attention is drawn not only to the inhomogeneous structure of the medium in the E region, but also to the Pedersen ray formation and the greater propagation range of this radio wave. The initial integral damping is nonzero. Since the elevation angle of this path is very small (5°), the wave propagates only slowly below 80 km where the absorption is great.

Figure 5 presents the results of calculations of the radio-wave propagation for 15:00 UT from a hypothetic transmitting station located at a point with the coordinates $\varphi = 72.6^\circ$ N, $\lambda = 68.1^\circ$ W; $\Phi = 84^\circ$ and $\Lambda = 5^\circ$. The station radiates radio waves along the meridian from the pole. Integral damping along each trajectory is shown by a dashed line. The trajectories calculated for the radio waves with three different frequencies are presented against the background of the electron-density isoline maps plotted along the radio-wave propagation paths in quiet conditions and in the main and recovery phases of geomagnetic storms.

The influence of the electron-density spatial inhomogeneities on the radio-wave propagation is clearly seen. The high density of the ionospheric plasma in quiet conditions of May 1 leads to the fact that the considered radio waves are reflected from the ionosphere at the altitudes of the lower part of the F_2 layer (170–180 km). In this case, the F_1 layer is absent. The appearance of this layer on May 2 is due to the diminishing of the plasma density in the high-latitude F region by about 25% and stipulates the electron-density irregularities along the radio-wave propagation path.

In the main phase of the geomagnetic storm, the range of the single-hop propagation path of a radio wave with the frequency $f = 8.5$ MHz and inclination angle $\alpha = 25^\circ$ increases considerably, and the radio-wave trajectory oscillates in the ionospheric valley between the F_1 and F_2 layers: the wave is doubly reflected from the F_2 layer and returns to the Earth (upper panel in Fig. 5*b*). The waveguide mechanism of propagation on some part of the radio-wave trajectory is also manifested here. The waves with the frequencies $f = 6.2$ MHz and $f = 7.2$ MHz are refracted in the F_1 layer and are reflected from the F_2 layer.

The most interesting results were obtained for the recovery phase of the storm (see Fig. 5*c*). Two of the considered radio waves, with the parameters $f = 6.2$ MHz, $\alpha = 25^\circ$ and $f = 7.0$ MHz, $\alpha = 30^\circ$ do not pass through the ionosphere. A considerable (by about 36%) drop of the electron number density and the appearance of the F_1 layer result in that two trajectories oscillate and have the largest length. In this case, the radio waves oscillate in a valley between the F_1 and F_2 layers. In turn, the wave with the frequency $f = 8.5$ MHz on May 3 passes through the ionosphere without reflection from it and undergoing

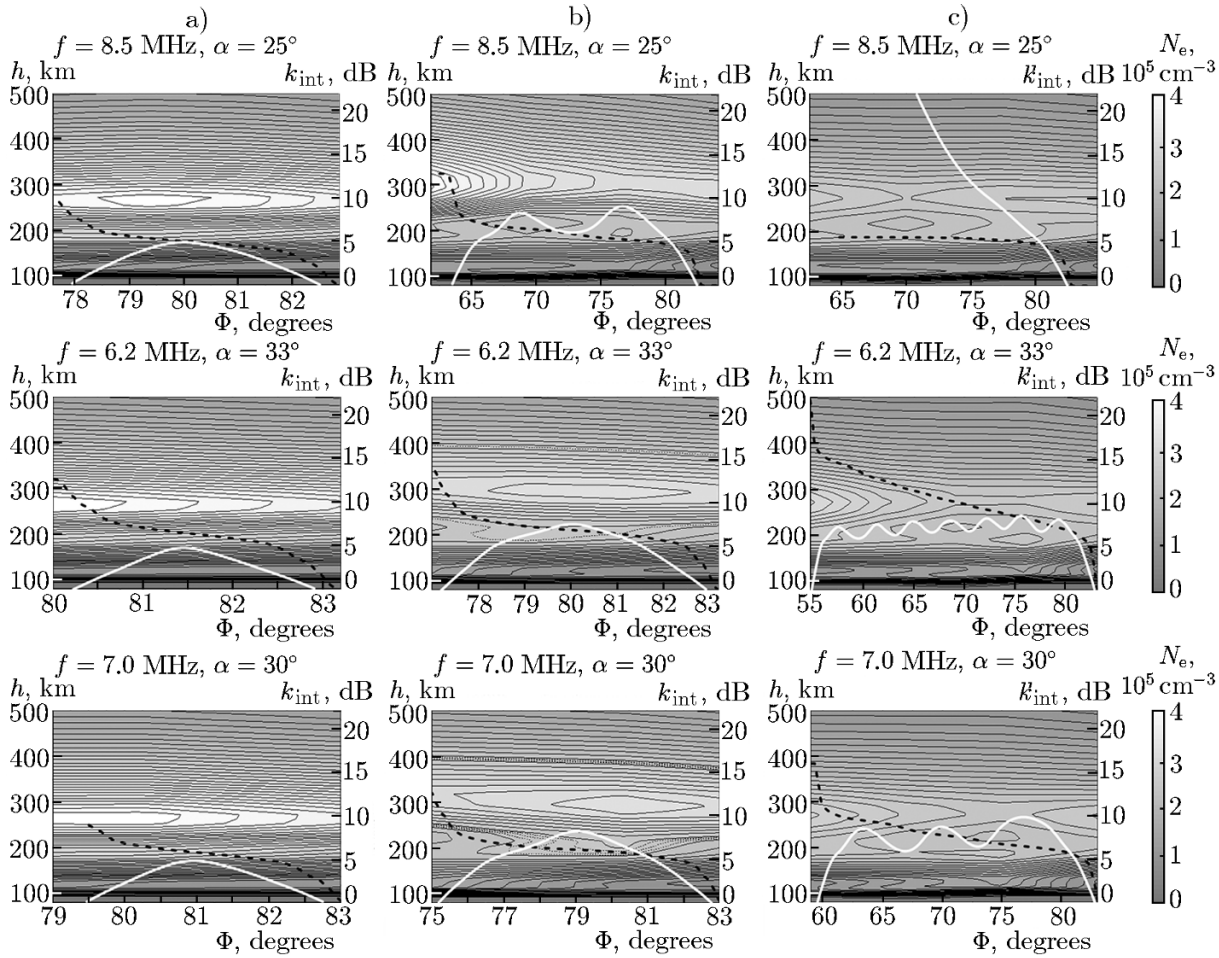

Fig. 5. Calculated trajectories (white lines) and integral dampings (dashed lines) of radio waves for a high-latitude ground-based radio station against the background of the electron density isolines constructed along the trajectories. The results are presented for quiet conditions (15:00 UT May 1, 2010, column *a* of the figures), in the main phase (15:00 UT May 2, 2010, column *b*) and the recovery phase of the storm (15:00 UT May 3, 2010, column *c*). The radio waves propagate from the right to the left.

only a slight refraction. It is well seen, especially on May 1, that as the operating frequency of the radio wave decreases, the absorption increases by 3 dB: with the same range of propagation from the transmitting station to the geomagnetic latitude $\Phi = 81^\circ$ the integral absorption coefficient $k_{\text{int}} \approx 7$ dB for the radio-wave frequency $f = 6.2$ MHz and $k_{\text{int}} \approx 4$ dB for $f = 8.5$ MHz.

We have studied the damping for the ordinary mode. The obtained results well agree with the existing concept, namely, that the extraordinary mode is reflected at lower altitudes and undergoes a stronger damping than the ordinary mode. It should be mentioned that in the model calculations we obtained a significant drop of the electron number density at the altitudes of the F_2 layer and insignificant changes in the F_1 layer in the recovery phase of the ionospheric storm. This is consistent with the conclusions drawn in [37] based on observation data of the incoherent scatter radars.

Figure 6 shows a differential damping along the trajectories of the radio waves with chosen frequencies, which was obtained for the same conditions at low and high latitudes. It is seen that the differential damping reaches the maximum values in the lower part of the E layer. Strong influence of the nondeflecting absorption, in which the ray deformation is small and the absorption is significant, is observed here. The wave propagates under conditions very different from reflection ($\omega \gg \omega_{\text{p}}$, where ω_{p} is the plasma frequency), and the real part of the refractive index is close to 1 [22]. Since during the geomagnetic storm the parameter

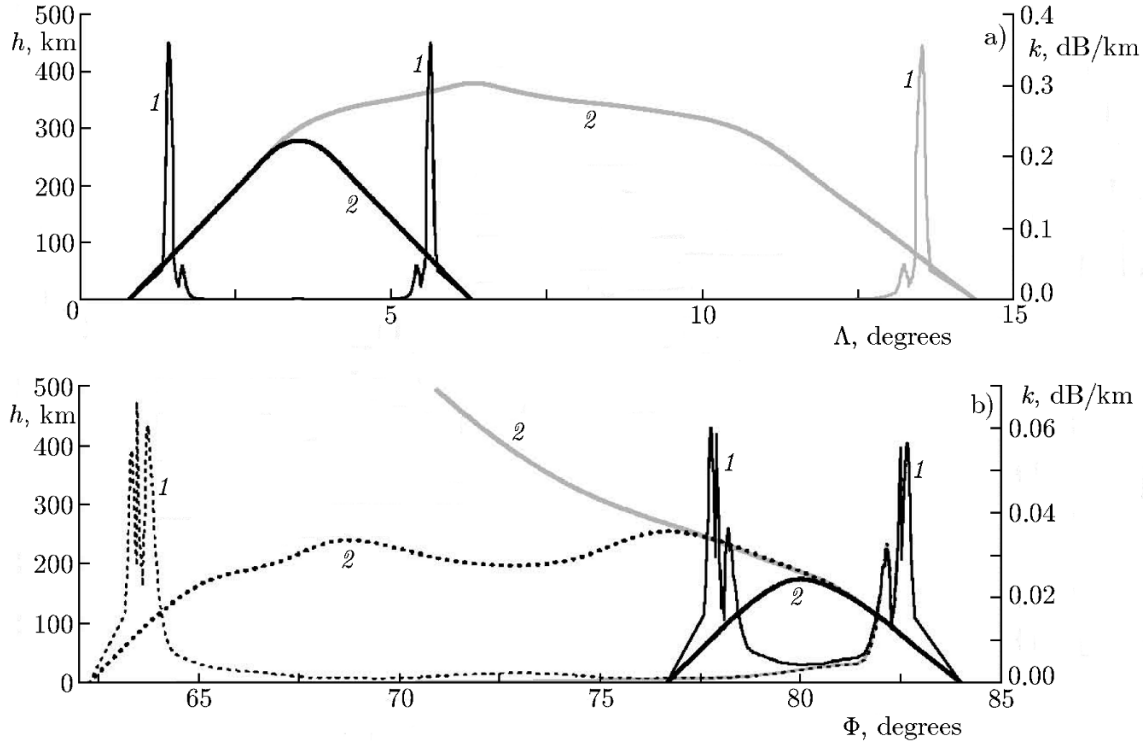

Fig. 6. Differential damping (curves *1*) along the trajectories (curves *2*) of radio waves with chosen frequencies in the period of a geomagnetic storm in the equatorial (panel *a*, $f = 2.86$ MHz) and high-latitude (panel *b*, $f = 8.5$ MHz) ionosphere. Black solid lines show the calculation results for May 1, dotted lines, for May 2, and gray lines, for May 3.

variations of the E layer are small compared with the variations in the F layer, the maximum differential damping appears to be about the same in order of magnitude in quiet conditions and during a geomagnetic storm. As the trajectories immerse into the ionospheric F layer, the real part of the refractive index falls, while the imaginary part rises. The vicinity of the turning point of the ray is characterized by a significant deformation of its trajectory, a decrease in the group velocity, and a rise in absorption. Such an absorption can be qualified as deflecting [22]. However, for the shown rays, this effect is weaker than the nondeflecting absorption. With the deeper immersion of these trajectories into the F_2 layer, the damping in the deflecting absorption region becomes stronger.

6. CONCLUSIONS

In this paper, to describe an inhomogeneous anisotropic medium during simulation of the HF radio-wave propagation we used GSM TIP, a global three-dimensional theoretical model of the thermosphere–ionosphere system. A series of numerical experiments on propagation of HF radio waves in the regions with multilayer ionospheric structure at high and low latitudes have been performed. Features of the trajectory formation in quiet conditions and during the May 2–3, 2010 geomagnetic storm are considered. It is shown that the presence of the F_1 layer in the high-latitude ionosphere and of the F_3 layer in the low-latitude ionosphere changes drastically the type of the radio-wave propagation.

The obtained calculation results made it possible to describe the reflection and refraction of HF radio waves from the electron-density inhomogeneities in the altitudinal, latitudinal, and longitudinal directions. Based on the obtained calculation results the conjecture is made that the oblique sounding ionograms can be used for a study of the spatial extent of the additional F_3 layer in the equatorial ionosphere and its variability during geomagnetic storms. The same can be said about the spatial extent of the F_1 layer in the

high-latitude ionosphere. The appearance of the F_1 layer in the high-latitude F region due to a significant decrease in the electron number density in the F_2 layer in the recovery phase of an ionospheric storm leads to the appearance of the radio-wave propagation channel, which increases significantly the range of their propagation. The damping of radio waves has the following features: the radio wave decays most strongly in the E region; despite the decrease in the electron number density during a geomagnetic storm, the absorption rises because of the increase in the radio-wave propagation range, the damping during a storm remains about the same in order of magnitude as in quiet conditions; the absorption rises with decreasing operating frequency.

The results can be used for interpretation of the actual oblique sounding ionograms obtained in different heliogeophysical environments.

The authors are grateful to Y. Sahai and N. A. Koren'kova for the experimental data and long fruitful collaboration.

This work was supported in part by the Council for Grants of the President of the Russian Federation (project MK-4866.2014.5, M. V. Klimenko and D. S. Kotova), Russian Foundation for Basic Research (project No. 14–05–00578, V. V. Klimenko), and the Program "Basic Problems in the Solar System Exploration" of the Presidium of the Russian Academy of Sciences.

REFERENCES

1. G. G. Vertogradov, V. P. Uryadov, and V. G. Vertogradov, *Radiophys. Quantum Electron.*, **48**, No. 6, 405 (2005).
2. K. A. Kutelev and V. I. Kurkin, in: *Proc. Int. All-Russia Sci. Conf. "The Propagation of Radio Waves," May 23–26, 2011, Yoshkar Ola* [in Russian], Vol. 1, p. 235.
3. A. T. Karpachev, G. A. Zhbankov, and V. A. Telegin, *Geomagn. Aeron.*, **53**, No. 6, 761 (2013).
4. D. Bilitza, *Radio Sci.*, **36**, No. 2, 261 (2001).
5. A. G. Miro, S. M. Cueto, K. Alazo, and M. Radicella, *Adv. Space Res.*, **39**, No. 5, 681 (2007).
6. M. V. Klimenko, V. V. Klimenko, K. G. Ratovsky, and L. P. Goncharenko, *Earth Planets Space*, **64**, No. 6, 433 (2012).
7. A. A. Namgaladze, Yu. V. Zubova, A. N. Namgaladze, et al., *Adv. Space Res.*, **37**, No. 2, 380 (2006).
8. G. Lu, L. P. Goncharenko, A. D. Richmond, et al., *J. Geophys. Res.*, **113**, No. 8, A08304 (2008).
9. N. Balan, K. Shiokawa, Y. Otsuka, et al., *J. Geophys. Res. A*, **115**, No. 2, A02304 (2010).
10. M. V. Klimenko, V. V. Klimenko, K. G. Ratovskii, and L. P. Goncharenko, *Geomagn. Aeron.*, **51**, No. 3, 364 (2011).
11. M. V. Klimenko, V. V. Klimenko, K. G. Ratovsky, et al., *Radio Sci.*, **46**, No. 3, RS0D03 (2011).
12. A. A. Namgaladze, Yu. N. Koren'kov, V. V. Klimenko, et al., *Geomagn. Aéron.*, **30**, No. 4, 612 (1990).
13. M. V. Klimenko, V. V. Klimenko, and V. V. Bryukhanov, *Geomagn. Aeron.*, **46**, No. 4, 457 (2006).
14. V. E. Zakharov and A. A. Chernyak, *Vestn. I. Kant RGU*, No. 3, 36 (2007).
15. V. E. Zakharov and D. S. Kotova, in: *Proc. XXIII All-Russia Sci. Conf. "The Propagation of Radio Waves," May 23–26, 2011, Yoshkar-Ola* [in Russian], Vol. 3, p. 340.
16. V. E. Zakharov and D. S. Kotova, *Radiotekhnika*, **2**, 87 (2013).
17. V. E. Zakharov and D. S. Kotova, *Vestn. I. Kant BFU*, No 4, 34 (2013).
18. M. Yu. Andreev, G. I. Mingaleva, and V. S. Mingalev, *Geomagn. Aeron.*, **47**, No. 4, 487 (2007).

19. M. Yu. Andreev, D. V. Blagoveshchensky, V. M. Vystavnoi, et al., *Geomagn. Aeron.*, **47**, No. 4, 502 (2007).
20. G. V. Kotovich, V. P. Grozov, A. G. Kim, et al., *Geomagn. Aeron.*, **50**, No. 4, 504 (2010).
21. Yu. A. Kravtsov and Yu. I. Orlov, *Geometrical Optics of Inhomogeneous Media* Springer–Verlag, Berlin, Heidelberg, Moscow (1990).
22. B. E. Bryunelli and A. A. Namgaladze, *Physics of the Ionosphere* [in Russian], Nauka, Moscow (1988).
23. D. S. Kotova, M. V. Klimenko, V. V. Klimenko, et al., in: *Proc. 18th Regional Conf. "The Propagation of Radio Waves," November 13–15, 2012, St. Petersburg* [in Russian], p. 72.
24. M. V. Klimenko, V. V. Klimenko, N. A. Korenkova, et al., in: *Proc. XXXV Annual Seminar "Physics of Auroral Phenomena" 28 February–02 March 2011, Apatity, Polar Geophys. Inst. KSC RAS*, p. 111.
25. M. V. Klimenko and V. V. Klimenko, *J. Atmos. Solar-Terr. Phys.*, **90–91**, 146 (2012).
26. E. Yu. Feshchenko and Yu. P. Maltsev, *Proc. XXVI Annual Seminar "Physics of Auroral Phenomena," 25–28 February 2003, Apatity, Polar Geophys. Inst. KSC RAS*, p. 59.
27. T. Iijima and T. A. Potemra, J. Geophys. Res., **81**, No. 34, 5971 (1976).
28. K. Snekvik, S. Haaland, N. Ostgaard, et al., *Ann. Geophys.*, **25**, 1405 (2007).
29. T. Kikuchi, K. K. Hashimoto, and K. Nozaki, *J. Geophys. Res. A*, **113**, No. 6, A06214 (2008).
30. J. J. Sojka, R. W. Schunk, and W. F. Denig, *J. Geophys. Res. A*, **99**, No. 11, 21341 (1994).
31. Y. Zhang and L. J. Paxton, *J. Atmos. Solar-Terr. Phys.*, **70**, Nos. 8–9, 1231 (2008).
32. D. S. Kotova, M. V. Klimenko, V. V. Klimenko, and V. E. Zakharov, *Vestnik I. Kant BFU*, No. 10 [in press].
33. N. Balan, I. S. Batista, M. A. Abdu, et al., *J. Geophys. Res. A*, **103**, No. 12, 29169 (1998).
34. M. V. Klimenko and V. V. Klimenko, *Geomagn. Aeron.*, **52**, No. 3, 321 (2012).
35. M. V. Klimenko, V. V. Klimenko, and A. T. Karpachev, *J. Atmos. Solar-Terr. Phys.*, **90–91**, 179 (2012).
36. C. H. Lin, A. D. Richmond, J. Y. Liu, et al., *J. Geophys. Res.*, **114**, No. 5, A05303 (2009).
37. A. V. Mikhailov and K. Schlegel, *Ann. Geophys.*, **21**, 583 (2003).